SUPER-HYDROPHOBIC DRAG REDUCTION IN TURBULENT CHANNEL AND PIPE FLOWS

Hyung Jae Lim

School of Mechanical and Nuclear Engineering,
UNIST
50 UNIST-gil, Ulsan 44919,
Korea
ihj465@unist.ac.kr

Jae Hwa Lee

School of Mechanical and Nuclear Engineering,
UNIST
50 UNIST-gil, Ulsan 44919,
Korea
jhlee06@unist.ac.kr

ABSTRACT

In the present study, direct numerical simulations (DNS) of turbulent pipe and channel flows with superhydrophobic surface (SHS) are performed to investigate the influence of the turbulence dynamics and the resultant drag reduction of the flows under similar conditions. SHSs at the wall are modeled in spanwise-alternating longitudinal regions with a boundary with no-slip and shear-free conditions, and the two parameters of the spanwise periodicity (P/δ) and SHS fraction (GF) within a pitch are considered. The skin friction drag for the pipe and channel flows over SHSs is continuously decreased with increases in P/δ and GF. However, the drag reduction (DR) rate in the pipe flows is greater than that in the channel flows with an accompanying reduction of the Reynolds stress. The enhanced performance of the DR for the pipe flow is attributed to the increased streamwise slip and weakened Reynolds shear stress contributions. In addition, a mathematical analysis of the spanwise mean vorticity equation suggests that the presence of a strong spanwise slip for the pipe flows makes a greater negative contribution of advective vorticity transport than the channel flows, resulting in a higher DR value.

INTRODUCTION

Many plants in nature including the lotus leaf exhibit the unusual wetting characteristic of superhydrophobicity. A SHS is obtained if air bubbles are entrapped within the small-scale surface features. It consists of surface roughness with shear-free layer over air-water interface, which corresponds to the Cassie-Baxter state (Cassie & Baxter 1944). Preservation of the interface enables the flow to slip along a shear-free surface, which leads to large skin-friction drag reduction (DR) in turbulent flows.

Recently, many numerical studies have been conducted to investigate flow modifications and DR mechanisms in turbulent flows by SHSs (Min & Kim 2004; Park et al. 2013). Min & Kim (2004) showed that the turbulent drag is reduced by streamwise slip over a SHS but increased by spanwise slip in a channel flow. Park et al. (2013) performed a DNS studies for a turbulent channel flow with longitudial SHS configuration. The results showed that turbulent DR up to 50% can be achieved for an equally spaced width between the SHS and the no-slip wall.

Despite the significant efforts in the work on flow physics and mechanisms in turbulent channel flows (and partially turbulent boundary flows) over SHSs, few researchers have attempted to examine the effects of SHSs on turbulent pipe flows, except for the experimental studies of Watanabe et al. (1999) and Lauga & Stone (2003).

In the present study, DNSs of turbulent pipe flows with SHSs are performed to investigate the distinctive flow characteristics in pipes over SHSs. In order to compare the results obtained from the pipe flows over SHSs, DNSs of turbulent channel flows with SHSs are also performed under similar conditions. The longitudinal SHSs in pipe and channel flows consist of repeating no-slip and shear-free conditions in the azimuthal (spanwise) direction. We initially estimate the DR rate in turbulent pipe and channel flows over SHSs with varying parameters of P/δ ($0.19 \le P/\delta \le 6.28$) and GF ($0.25 \le GF \le 0.75$). For a better understanding of the mechanisms responsible for the differences in the DR rates between pipe and channel flows, mathematical analyses using a streamwise mean momentum equation (Fukagata et al. 2002) and a spanwise mean vorticity equation (Yoon et al. 2016) are conducted.

NUMERICAL DETAILS

For incompressible fully developed turbulent pipe and channel flows over a smooth wall, the Navier-Stokes and continuity equations in cylindrical coordinates and Cartesian coordinates are employed as governing equations. For the cylindrical coordinates, the notation r is the radial coordinate measured along the pipe axis; x denotes the flow axial direction; θ is the azimuthal coordinate; and u_r, u_x, and u_θ are the corresponding velocity components. For the Cartesian coordinates, x, y and z denote the streamwise, wall-normal, and spanwise coordinates, respectively, and u, v and w denote the corresponding velocity components. For the purpose of an analogy between pipe and channel flows, the axial coordinate in the cylindrical coordinates is defined as $x=x$, the wall-normal coordinate as $y=1-r$, and the spanwise coordinate as $z=r\theta$ (Monty et al. 2007; Wu et al. 2012). In addition, it is useful to define the analogous velocity components $u=u_x$, $v=-u_r$ and $w=u_\theta$. In order to non-dimensionalize the governing equations, the maximum velocity of the fully developed laminar profile (U_{co}) and the outer length scale (δ) for each flow are used, where δ is the channel half height or pipe radius. The equations are integrated over time using the fractional step method along with the implicit velocity decoupling procedure (Kim et al. 2002). Block LU decomposition based on approximate factorization is applied to achieve both

velocity-pressure decoupling and the decoupling of the intermediate velocity components. In this approach, the terms are initially discretized in time using the Crank-Nicholson method, after which the coupled velocity components are solved without iteration. All terms are resolved using a second-order central difference scheme in space with a staggered mesh.

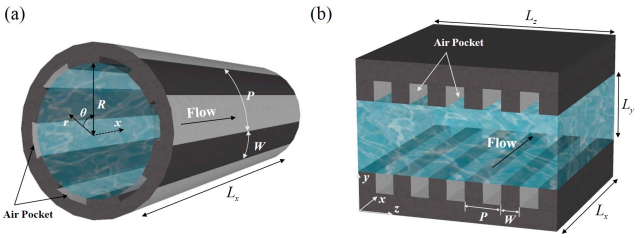

Figure 1. Schematic of turbulent (a) pipe and (b) channel flows over super-hydrophobic surfaces. The walls consist of spanwise-alternating longitudinal surfaces with shear-free and no-slip conditions.

In the present study, the SHSs are assumed to be placed on limited longitudinal surfaces for simplicity (Figure 1). A SHS with a width of P-W is repeatedly arranged in the spanwise direction with a no-slip surface of width W (black), and the SHSs in channel are positioned at both the top and bottom walls. Two sets of parametric studies are considered: the pitch (P/δ) and the gas fraction (GF=(P-W)/P). To facilitate a comparison between the pipe and channel flows, the computational domain (L_x x L_y x L_z) for each flow is equal to 6δ x 2δ x 2$\pi\delta$ with a corresponding mesh size of 192 x 129 x 256. Non-uniform grid distributions are employed in the wall-normal direction using a hyperbolic tangent function and a uniform grid distribution in both the streamwise and spanwise directions. Periodic boundary conditions are applied along the streamwise and spanwise directions. On the bottom and top walls, the boundary condition at the wall is given as alternating shear-free (($\partial u/\partial y)_w$=0 and ($\partial w/\partial y)_w$=0) and no-slip conditions in the spanwise direction (Philip 1972). The mean pressure gradient is dynamically adjusted to maintain a mass flow rate constant.

The initial Reynolds numbers for the pipe and channel flows are Re_{co}(=$U_{co}\delta/\nu$)=5300 and 4200, respectively, and the corresponding friction Reynolds number for each flow is $Re_{\tau o}$(=$U_{\tau o}\delta/\nu$)=180 based on the friction velocity of a regular no-slip pipe and channel walls ($U_{\tau o}$), where ν is the kinematic viscosity of the fluid. The subscript 'o' indicates the value for a regular pipe and channel flows. The superscripts + refer to quantities normalized by the initial friction velocity $U_{\tau o}$, and capital letters depict the temporally and spatially averaged (on the horizontal plane) statistics.

Because the SHS is positioned in a limited area on the entire wall, it is natural to expect spatial variations of the flow characteristics statistically, thus requiring phase-averaging in the spanwise direction. Phase-averaging operator leading to triple decomposition of the velocity as suggested by Reynolds & Hussain (1972). Coherent fluctuations are defined by the Jelly et al. (2014).

RESULTS AND DISCUSSION

Skin-friction Drag

In order to examine the effects of SHSs on turbulent skin-friction drag, the variations of the skin friction drag coefficient (C_f) in fully developed turbulent pipe and channel flows are plotted in Figure 2 under varying P/δ and GF values. The drag is estimated as the ratio of the plane-averaged skin-friction coefficients to values (C_{fo}) obtained from regular no-slip pipe and channel flows. A direct comparison of our data with the DNS data from Park et al. (2013) for fully developed channel flows over SHSs shows good agreement, providing evidence of the accuracy and reliability of our simulations. In Figure 2(a), as P/δ increases for fixed GF value of 0.25, 0.5 and 0.75, the normalized drag for the pipe and channel flows over SHSs shows a continuous decrease up to P/δ=6.28. The most interesting observation in the figure is that maximum turbulent DR rate in the pipe flows is larger than that in the channel flows for all P/δ. In particular, the maximum difference in the DR rate between the pipe and channel flows was found to be as high as 8% at P/δ=6.28 for GF=0.5. In Figure 2(b), as GF increases for fixed values of P/δ=0.19 and 6.28, the drag is significantly decreased up to 50% and 10% for flows over SHSs at GF=0.75. Compared to the variation shown in Figure 2(a), the drag with varying GF exhibits a nearly linear decrease for a fixed P/δ. Although the drag for a small value of P/δ=0.19 shows a negligible difference between turbulent pipe and channel flows over the SHSs, that for a large value of P/δ indicates a large drag difference between the two cases. Because the turbulent DR for P/δ=6.28 with an increase in GF is significant for both flows (Figure 2b), the difference in the drag between the pipe and channel flows over SHSs is smaller at GF=0.75 than at GF=0.5.

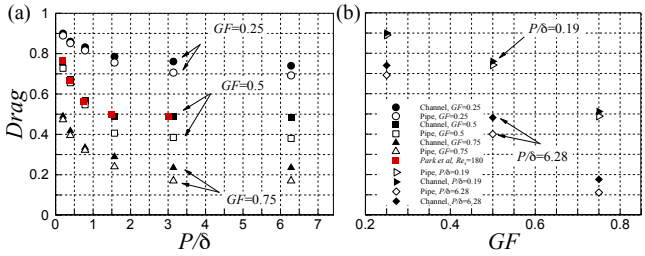

Figure 2. Variation of the normalized drag as a function of (a) P/δ for GF=0.25, 0.5 and 0.75 and (b) GF for P/δ=0.19 and 6.28 in turbulent pipe and channel flows over SHSs. Open and closed symbols indicate the pipe and channel data. Red squares is visible for validation with the channel data of Park et al. (2013).

Turbulent Statistics

The turbulent statistics of the pipe and channel flows over SHSs are analyzed to investigate the influence of the SHSs on the flow characteristics. Figures. 3(a) and (b) show the mean streamwise velocity profiles normalized by the initial friction velocity ($U_{\tau o}$) when P/δ and GF vary. Here, GF and P/δ are fixed at 0.5 and 6.28 due to the large drag difference between the pipe and channel flows in Figure 2. An inspection of the mean velocity profiles showed that the mean velocity shear clearly decreases

with an increase in P/δ and GF. In addition, as DR increased, the near-wall velocities were continuously shifted upward due to the streamwise slip velocity and the pipe flows had higher streamwise slip velocities than those of the channel flows.

Figures. 3(c) and (d) illustrate variation of streamwise slip velocity at the wall (U_s) normalized by $U_{\tau o}$ when P/δ and GF vary. As P/δ increases for the fixed GF values of 0.25, 0.5 and 0.75 in Figure 3(c), the normalized streamwise slip velocity for the pipe and channel flows over SHSs increases continuously up to P/δ=6.28, and the values in the pipe flows are larger than those in the channel flows for all P/δ. However, compared to the drag difference shown in Figure 2, it is clear that the difference in the slip velocity between the pipe and channel flows is similar for all P/δ with varying GF. The implication of the present observation is that the drag is not mostly determined by the streamwise slip velocity at the wall for both flow types. Other effects, such as the modification of the turbulence dynamics, may play an important role in generating the drag.

In Figure. 4, profiles of the Reynolds stresses normalized by $U_{\tau o}$ are shown with the variances of P/δ (left) and GF (right) for the pipe and channel flows over SHSs. When GF=0.5, increasing P/δ leads to a continuous reduction of the streamwise Reynolds stress far from the wall for the pipe and channel flows. However, in the very-near-wall region, i.e., y^+<5, the streamwise-normal stress is enhanced with an increase in P/δ (P/δ<3.14) due to the increased streamwise slip velocity, whereas the stress values are decreased when P/δ≥3.14. For the wall-normal and spanwise turbulent stresses and Reynolds shear stress, the magnitudes for y^+>5 continuously decrease up to P/δ=1.56, while they slightly increase when P/δ≥3.14. The spanwise components of the Reynolds stresses near the wall (y^+<5) are continuously amplified with an increase in P/δ. As expected, the profiles of the Reynolds stresses for the pipe and channel flows indicate that the turbulence for the pipe flows is greatly suppressed in the outer layer. However, the near-wall turbulence activity for the pipe flow is enhanced due to the larger streamwise slip velocity for the pipe flow (Figure 3). In Figure 4(b), as GF increases for a fixed P/δ, the Reynolds stresses decrease continuously in the outer layer, whereas the near-wall streamwise and spanwise normal Reynolds stresses are increased. In our study, although the Reynolds stresses are normalized by $U_{\tau o}$.

The spanwise Reynolds stress in the near-wall region continuously increases, as shown in Figure 4(e). In order to examine the increase of the spanwise Reynolds stress near the wall, the probability density function (p.d.f.) of the instantaneous spanwise slip velocity at the wall (w_s) as a function of P/δ and GF is devised, as shown in Figure. 5. Because the plane-averaged mean spanwise velocity is zero due to the reflectional symmetry of the velocity component about the origin, it is therefore useful to plot the p.d.f. of the instantaneous spanwise velocity with consideration of its sign. As expected, the value of w_s increases with the increases in P/δ and GF for the pipe and channel flows, leading to greater spanwise Reynolds stresses near the wall with increases in P/δ and GF. In addition, a higher value of w_s is observed for pipe flows with a longer tail.

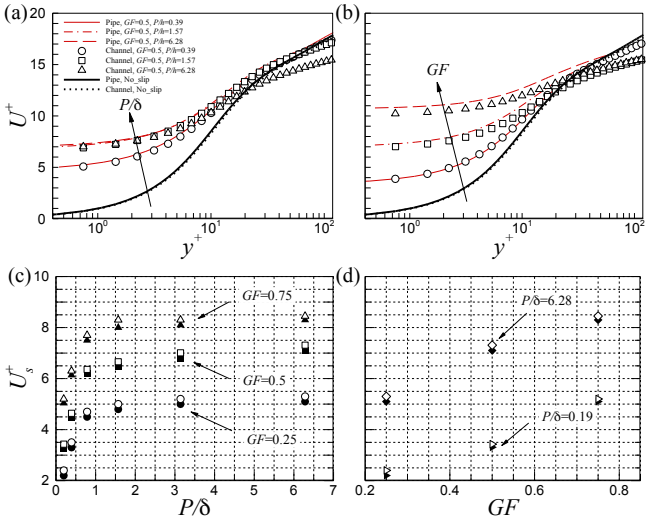

Figure 3. Mean streamwise velocity profiles as a function of (a) P/δ for GF=0.5 and (b) GF for P/δ=6.28. Variation of the streamwise slip velocity at the wall (U_s) normalized by $U_{\tau o}$ as a function of (c) P/δ for GF=0.5 and (d) GF for P/δ=6.28. The legends for (c) and (d) are identical to those in Figure 2.

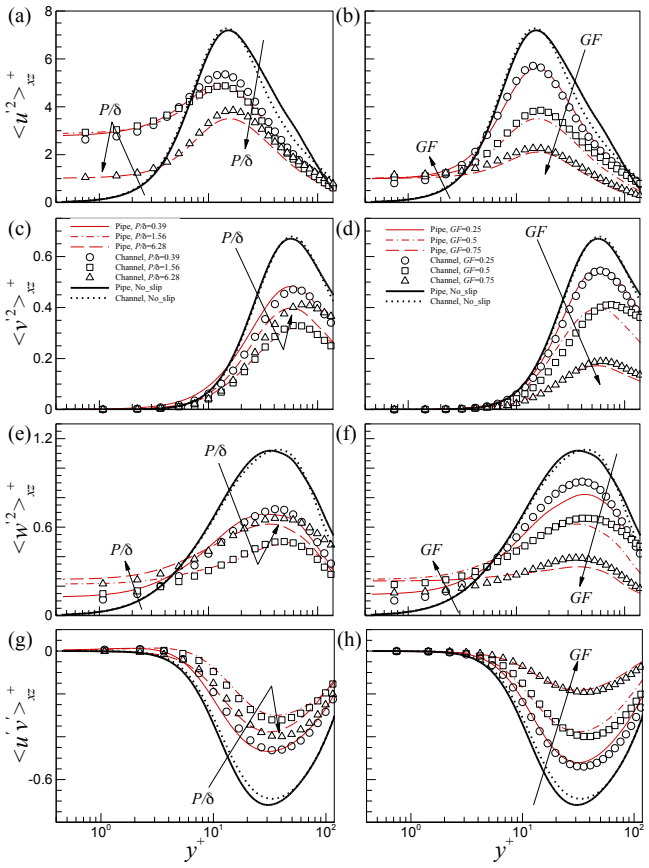

Figure 4 Reynolds stress profiles in turbulent pipe and channel flows over SHSs as a function of (a, c, e, g) P/δ for GF=0.5 and (b, d, f, h) GF for P/δ=6.28. (a, b) streamwise, (c, d) wall-normal, (e, f) spanwise normal stresses, and (g, h) the Reynolds shear stress.

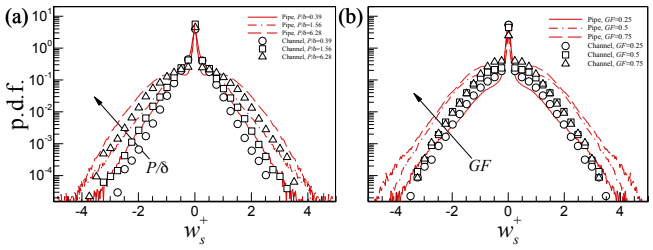

Figure 5. Probability density functions (p.d.f.) of the instantaneous spanwise slip velocity at the wall (w_s) as a function of (a) P/δ for GF=0.5 and (b) GF for P/δ=6.28.

Skin-friction Budget

We estimate the componential contributions of the skin friction drag to identify different dynamical effects in pipe and channel flows over SHSs (Fukagata et al. 2002), hereafter referred to as FIK. The FIK identity is derived by taking the triple integral of the streamwise component of the Reynolds Averaged Navier-Stokes equation along the wall-normal direction. The final form of the FIK identity for a pipe flow with azimuthal inhomogeneity can be summarized as follows (plane-averaged form):

$$< C_f >_{xz}^{sum} = < C_f >_{xz}^{lam} + < C_f >_{xz}^{R12} + < C_f >_{xz}^{SHS} \quad (1)$$

$$< C_f >_{xz}^{lam} = \left\langle \frac{8}{U_b Re_b}\left(1-\frac{U_s}{U_b}\right) \right\rangle_{xz} \quad (2)$$

$$< C_f >_{xz}^{R12} = -\left\langle \frac{8}{U_b^2}\int_0^1 r\langle u'v'\rangle dr \right\rangle_{xz} \quad (3)$$

$$< C_f >_{xz}^{SHS} = -\left\langle \frac{4}{U_b^2}\int_0^1 (r^2-1)\left(\overline{\overline{\langle v\rangle \frac{\partial \langle u\rangle}{\partial y}}} + \overline{\overline{\langle w\rangle \frac{\partial \langle u\rangle}{\partial z}}} \right) rdr \right\rangle_{xz}$$
$$-\left\langle \frac{4}{U_b^2}\int_0^1 (r^2-1)\left(\frac{\partial \overline{\overline{\langle u'w'\rangle}}}{\partial z} \right) rdr \right\rangle_{xz}$$
$$+\left\langle \frac{4}{U_b^2 Re_b}\int_0^1 (r^2-1)\frac{\partial^2 \overline{\overline{\langle u\rangle}}}{\partial z^2} rdr \right\rangle_{xz} \quad (4)$$

, where Re_b is the Reynolds number based on the bulk mean velocity (U_b), $\overline{\overline{\langle\cdot\rangle}} = \langle\cdot\rangle - \int_0^1 \langle\cdot\rangle dy$. Similarly, the FIK identity for channel flows over SHSs can be calculated the same manner (Jelly et al. 2014).

Eq. (1) indicates that the contribution to the skin friction drag comes from three different contributions. The first (Eq. 2) and second (Eq. 3) terms indicate the corresponding contributions of the local streamwise slip velocity (laminar contribution) and the Reynolds shear stress. All additional terms can be lumped into the third term (Eq. 4), which represents the wall-normal convection contribution, the spanwise force due to the spanwise gradients of the spanwise Reynolds stress, and the spanwise diffusion of the streamwise velocity. Figure. 6 shows the contribution of plane-averaged FIK identity towards turbulent skin friction drag normalized by the skin friction drag of regular no-slip pipe and channel flows as a function of P/δ for fixed GF values of 0.25, 0.5 and 0.75. The contribution of the streamwise slip velocity accounted for approximately 50% of the difference (4%) in the drag between the pipe and channel flows regardless of the value of P/δ for all GF, and the Reynolds shear stress contribution accounted for 1~4% of the difference in the drag as P/δ varied. The zero contribution of the third term (Figure 6d) is due to the negative contribution of wall-normal convection towards the skin friction drag due to the presence of secondary motion and the edge effect of the shear-free region, although the phase-averaged FIK identity over the no-slip plane can positively reproduce the skin friction drag.

In addition to the FIK identity above, a relationship between the skin friction drag and turbulent vortical motions can be introduced by performing triple integration of the spanwise component of the mean vorticity equations with respect to the wall-normal direction for pipe flows, as follows (Yoon et al. 2016),

$$\langle C_f \rangle_{xz}^{sum} = \underbrace{\left\langle \int_0^1 2r\langle v'\omega_z'\rangle dr \right\rangle}_{\langle C_{f1}\rangle_{xz}} + \underbrace{\left\langle \int_0^1 2r\langle -w'\omega_y'\rangle dr \right\rangle}_{\langle C_{f2}\rangle_{xz}} + \underbrace{\left\langle \frac{1}{Re_\tau}\frac{\partial \Omega_z}{\partial r}\Big|_{r=1} \right\rangle}_{\langle C_{f3}\rangle_{xz}}$$
$$+ \underbrace{\left\langle \frac{1}{Re_\tau}\int_0^1 \Omega_z dr \right\rangle}_{\langle C_{f4}\rangle_{xz}} + \underbrace{\left\langle \int_0^1 (r^2-1)\langle I_z\rangle dr \right\rangle}_{\langle C_{f5}\rangle_{xz}} + \underbrace{\left\langle \frac{1}{Re_\tau}\int_0^1 r\frac{\partial \Omega_z}{\partial r} dr \right\rangle}_{\langle C_{f6}\rangle_{xz}}, \quad (5)$$

Similarly, the channel flows over SHSs can be calculated the same manner.

The FIK identity with the velocity-vorticity correlation showed that the difference in the skin friction drag between the pipe and channel flows is mostly due to the significant discrepancy in the contributions of the advective vorticity transport terms (C_{f1}). Because a secondary flow in the form of a pair of counter-rotating vortices plays an important role in generating turbulent momentum transport, the larger negative contribution of the advective vorticity transport in the pipe flows than in the channel flows provides evidence of the presence of stronger secondary flows in pipe flows, consistent with the observation pertaining to the spanwise slip velocity. Contrary to the finding that the increased rates of the streamwise slip velocity for the pipe and channel flows were similar, the higher rate of change for the drag and spanwise slip velocity in the pipe flows as compared to the channel flows as P/δ varied indicated that the spanwise slip velocity for the turbulent flows over SHSs is also an important contributor to the reduction of the skin friction drag. The larger spanwise slip velocity as P/δ and GF vary in the pipe flows was consistent with the greater decrease of the Reynolds shear stress contribution in the pipe flows, as the spanwise slip weakens the near-wall turbulence with less of a wall-normal gradient of the spanwise velocity.

SUMMARY AND CONCLUSIONS

In the present study, we performed DNSs of fully developed turbulent pipe and channel flows with SHSs at the wall. A comparison of a superhydrophobic turbulent DR between turbulent pipe and channel flows showed that as P/δ and GF increase, the difference in the normalized drag between the pipe and channel flows increases. In particular, when GF=0.5, the difference in the DR was shown to be maximized up to 8% for a large P/δ. all of the Reynolds stresses in the outer layer decrease

continuously, as P/δ and GF increase. Compared to small P/δ, turbulence for large P/δ over the no-slip wall is not significantly affected by the shear-free wall, and thus there are observed active turbulent motions with large Reynolds stresses. The Reynolds stresses in the pipe flow are smaller than those in the channel-

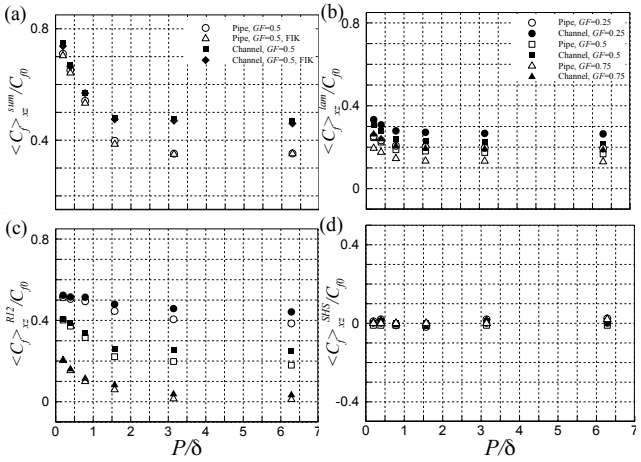

Figure 6 Variation of terms in the plane-averaged FIK identity as a function of P/δ for fixed GF values of 0.25, 0.5 and 0.75 in turbulent pipe and channel flows over SHSs.

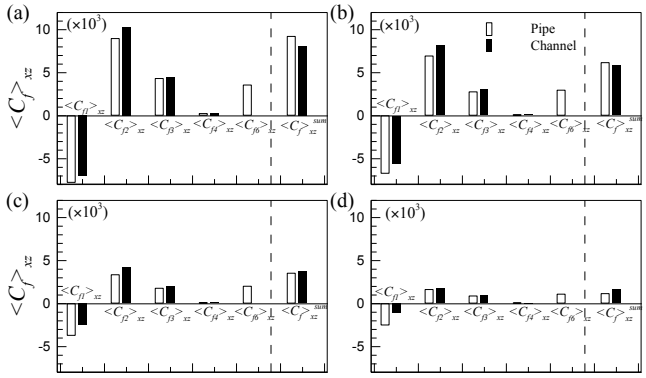

Figure 7 Skin friction drag for pipe and channel flows over SHSs calculated from the FIK identity with velocity-vorticity correlation: (a) no-slip, (b) GF=0.5, P/δ=0.39, (c) GF=0.5, P/δ=6.28 and (d) GF=0.75, P/δ=6.28.

-flow, consistent with previous observation in drag reduction rate. By mathematical analysis using streamwise mean momentum equation (Fukagata et al. 2002), The contribution of the streamwise slip velocity accounted for approximately 50% of the difference (4%) in the drag between the pipe and channel flows regardless of the value of P/δ for all GF, and the Reynolds shear stress contribution accounted for 1~4% of the difference in the drag as P/δ varied. Furthermore, the FIK identity with the velocity-vorticity correlation showed that the difference in the skin friction drag between the pipe and channel flows is mostly due to the significant discrepancy in the contributions of the advective vorticity transport terms.

ACKNOWLEDGEMENT

This research was supported by Basic Science Research Program through the National Research Foundation of Korea (NRF) funded by the Ministry of Education (NRF-2014R1A1A2057031).

REFERENCES

Cassie, A. & Baxter, S. 1944Wettability of porous surfaces. *Trans. Faraday Soc.* **40**, 546–551.

Fukagata, K., Iwamoto, K. & Kasagi, N. 2002 Contribution of Reynolds stress distribution to the skin friction in wall-bounded flows. *Phys. Fluids* **14**, L73–L76.

Jelly, T. O., Jung, S. Y. & Zaki, T. A. 2014 Turbulence and skin friction modification in channel flow with streamwise-aligned superhydrophobic surface texture. *Phys. Fluids* **26**, 095102.

Kim, K., Baek, S.-J. & Sung, H. J. 2002 An implicit velocity decoupling procedure for the incompressible Navier-Stokes equations. *Intl J Numer Meth Fluids* **38**, 125-138.

Lauga, E. & Stone, H. A. 2003 Effective slip in pressure-driven Stokes flow. *J. Fluid Mech*. **489**, 55–77.

Min, T. & Kim, J. 2004 Effect of superhydrophobic surfaces on skin-friction drag. *Phys. Fluids* **16**, L55.

Park, H., Park, H. & Kim, J. 2013 A numerical study of the effects of superhydrophobic surface on skin-friction drag in turbulent channel flow. *Phys. Fluids* **25**, 110815.

Philip, J. R. 1972 Flows satisfying mixed no-slip and no-shear conditions. *Z. Angew. Math. Phys.* **23**, 353-372.

Reynolds, W. C., & Hussain, A. K. M. F. 1972 The mechanics of an organized wave in turbulent shear flow. Part 3. Theoretical models and comparisons with experiments. *J. Fluid Mech.* **54(02)**, 263-288.

Watanabe, K., Yanuar & Udagawa, H. 1999 Drag reduction of Newtonian fluid in a circular pipe with a highly water-repellent wall. *J. Fluid Mech*. **381**, 225–238.

Yoon, M., Ahn, J., Hwang, J., & Sung, H. J. 2016. Contribution of velocity-vorticity correlations to the frictional drag in wall-bounded turbulent flows. *Phys. Fluids* **28(8)**, 081702.